
Explaining Temporal Effects in Sepsis Prediction

Anonymous Author(s)

Affiliation
Address
email

Abstract

1 Sepsis prediction models remain opaque to clinicians which hinder clinician adoption: without understanding why a patient is flagged as high-risk, accurate predictions may be ignored, delaying critical intervention. Existing explainability
2 methods focus on feature importance and often overlook timing, thus failing to
3 capture the temporal influences inherent in time-series data. We propose Positional
4 Explanation, which separates attributions into feature content and its position to
5 highlight temporal effects, enabling clinicians to identify early warning indicators
6 and monitor for specific physiological changes at critical time windows before sepsis
7 develops. Applied to GPT-2 and Mamba models finetuned for sepsis prediction
8 on PhysioNet and MC-MED benchmarks, our method achieves higher faithfulness
9 scores and reveals temporal patterns in sepsis progression that existing techniques
10 miss, potentially enabling earlier detection and improved patient outcomes.
11
12

13 1 Introduction

14 Sepsis is a leading cause of hospital mortality, primarily because it is often detected after irreversible
15 organ damage [Seymour et al., 2016]. While deep learning models can predict its onset with high
16 accuracy, they typically only signal that the risk of sepsis is high, not why [Yuan et al., 2020, Bomrah
17 et al., 2024]. This leaves a ‘lab-to-bedside’ gap: without understanding the subtle physiological
18 patterns that precede overt signs, clinicians cannot act on predictions early enough to save lives.

19 Explainable AI (XAI) methods have the potential to bridge this gap. Beyond fostering trust, these
20 methods can turn predictive models into tools for clinical discovery [Wong et al., 2021, Shashikumar
21 et al., 2021, Adams et al., 2022]. By illuminating the reasoning behind a model’s predictions, these
22 methods can foster the clinical trust necessary for early intervention [Wong et al., 2021, Shashikumar
23 et al., 2021, Adams et al., 2022]. However, existing explanation methods are fundamentally
24 misaligned with the temporal nature of diseases like sepsis.

25 Sepsis is a disease of trajectory; a patient’s physiological trend over time—the when—is often more
26 diagnostically significant than any single measurement—the what [Zhu et al., 2023]. An elevated
27 heart rate, for instance, may signal danger when it appears early and persists, yet prove benign if
28 transient. Despite this temporal criticality, existing explanation methods like LIME [Ribeiro et al.,
29 2016] and Integrated Gradients [Sundararajan et al., 2017] only quantify feature importance, leaving
30 temporal dynamics unexplained.

31 This blind spot reflects a broader challenge in machine learning. Recent studies have shown that
32 modern deep learning architectures are highly sensitive to input order; even reordering elements in
33 a sequence can substantially change a model’s output [Liu et al., 2024, Wang et al., 2024]. This
34 positional sensitivity in general sequence modeling directly parallels the temporal sensitivity in
35 time-series applications like sepsis prediction. Yet current explanation methods cannot address the
36 fundamental question underlying temporal diagnosis: “Is this feature important because of its value,
37 or because of its timing?” Based on this, we argue that to bridge the trust gap, a clinically adequate

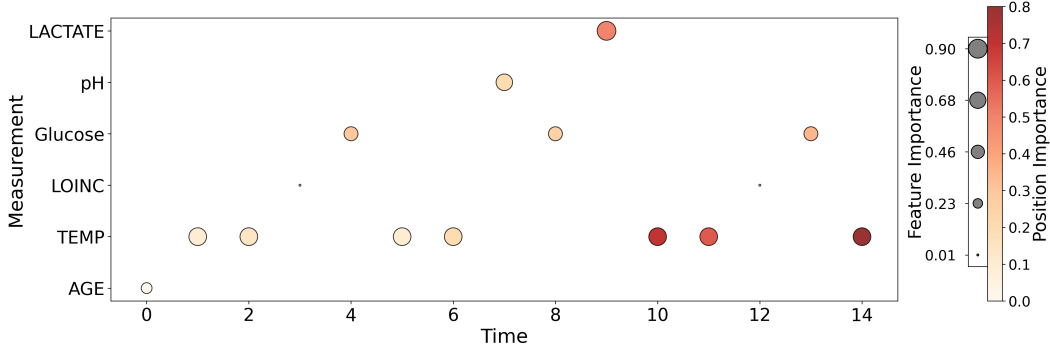


Figure 1: Feature content attribution score $\alpha^{(\text{feature})}$ and absolute position attribution score $\alpha^{(\text{position})}$ for a representative example from the PhysioNet dataset. The visualization demonstrates that feature importance and positional importance differ substantially: while TEMP measurements maintain consistent feature content attribution across time steps, their positional importance increases over time, indicating that there is a temporal effect of TEMP measurement importance for sepsis prediction.

38 explanation must be able to separate the importance of ‘what’ (the feature itself) from ‘when’ (its
 39 temporal effect).

40 To address this, we introduce **Positional Explanation**, a framework that decomposes the standard
 41 attribution score into two distinct components: (1) a **feature content score** reflecting its intrinsic
 42 clinical value, and (2) a **position score** that quantifies the importance of the temporal effect. We apply
 43 our framework to Mamba [Gu and Dao, 2024] and GPT-2 [Radford et al., 2019] models finetuned
 44 for early sepsis prediction, using the EHR data from PhysioNet [Reyna et al., 2020] and MC-MED
 45 [Kansal et al., 2025]. To summarize, our contributions are:

46 • We formalize a framework called Positional Explanation that decomposes attribution scores into
 47 feature and position effects for time-series data.
 48 • We demonstrate through quantitative experiments that our decomposition provides more faithful
 49 explanations than existing explanation methods.
 50 • We show that our framework identifies clinically relevant, time-dependent biomarkers missed by
 51 existing methods, offering more actionable insights for clinicians.

52 2 Related Work

53 The drive to deploy predictive models in high-stakes clinical settings has led to a surge in research on
 54 explainable AI (XAI) for medical time series data [Tonekaboni et al., 2019, Topol, 2019]. The primary
 55 goal is to move beyond black-box predictions and provide clinicians with transparent, trustworthy,
 56 and actionable insights, thereby fostering adoption and facilitating model auditing. This need is
 57 particularly acute in sepsis prediction, where timely and interpretable predictions can directly impact
 58 patient outcomes.

59 The dominant paradigm for explaining time-series models relies on post-hoc feature attribution
 60 methods that generate saliency maps. Foundational techniques like LIME [Ribeiro et al., 2016],
 61 SHAP [Lundberg and Lee, 2017], and Integrated Gradients [Sundararajan et al., 2017] are commonly
 62 adapted to clinical time series including sepsis prediction, assigning an importance score to each
 63 feature at each timestep [Shickel et al., 2017, Lauritsen et al., 2020]. More recent work has sought
 64 to create methods tailored specifically for time series, such as TimeSHAP [Bento et al., 2021] or
 65 Dynamask [Crabbé and van der Schaar, 2020], which aim to produce more faithful explanations
 66 by considering the temporal nature of the data. Other approaches generate explanations through
 67 counterfactuals—identifying what minimal changes to an input sequence would alter the model’s
 68 prediction [Goyal et al., 2021, Ismail and Günemann, 2021].

69 However, a critical and unaddressed limitation unites these methods: they treat each feature-timepoint
 70 observation as an atomic unit. Consequently, the resulting attribution score—whether from a saliency
 71 map or a counterfactual—fundamentally conflates the importance of a feature’s content (the ‘what’)

72 with the importance of its temporal position (the ‘when’). For instance, in sepsis prediction, a standard
 73 explanation cannot distinguish whether an elevated lactate reading is flagged because lactate is a
 74 clinically significant marker of sepsis or because the model has learned a spurious recency bias where
 75 any observation in the final timestep is overweighted [Jain and Wallace, 2019, Ismail and Gündemann,
 76 2021]. This entanglement prevents a deeper audit of the model’s temporal reasoning, which is crucial
 77 for sepsis where the timing of physiological changes carries diagnostic significance.

78 This limitation is particularly striking given that modern sequence models, like the Transformer and
 79 Mamba, explicitly separate content and position through distinct token and positional embeddings
 80 [Vaswani et al., 2017, Gu and Dao, 2024]. While the model’s architecture maintains this separation—enabling it to learn both what features matter and when they matter—the explanation methods
 82 used to interpret them do not. This is especially problematic for sepsis onset prediction, which is
 83 fundamentally a temporal problem where understanding both the clinical markers and their temporal
 84 evolution is essential for meaningful interpretation.

85 3 Positional Explanation

86 Feature attribution is the dominant paradigm for interpreting model behavior, assigning an importance
 87 score to each input feature [Doshi-Velez and Kim, 2017]. Existing methods answer the question:
 88 “Which features contributed most to the model’s prediction?” However, they conflate feature content
 89 and positional effects, making it impossible to separate a feature’s semantic contribution from the
 90 effect of its position.

91 Formally, consider a model $f : \mathcal{X} \rightarrow \mathcal{Y}$ and a single input instance $x \in \mathcal{X}$. Each component x_i of x
 92 represents a specific feature of that input. An **explainer**, g , is a function that maps the model and
 93 input instance to an attribution vector:

$$\alpha = g(f, x) \in \mathbb{R}^d \quad (1)$$

94 where d is the dimensionality of x . The entry α_i measures the combined influence of the i -th feature
 95 content x_i and its position on the model’s prediction $f(x)$.

96 As shown in Equation (1), existing explainer g only requires f, x as input, with no positional in-
 97 formation. Consequently, existing methods cannot reveal positional effects. Perturbation-based
 98 (LIME [Ribeiro et al., 2016], SHAP [Lundberg and Lee, 2017]) and gradient-based methods (Inte-
 99 grated Gradients [Sundararajan et al., 2017]) attribute importance solely to feature values at fixed
 100 positions, while decomposition-based approaches (FullGrad [Srinivas and Fleuret, 2019]) assign
 101 relevance to features at their original locations. In all cases, attributions reflect feature influence only.

102 **Positional Explanation Framework.** We propose *Positional Explanation*, a framework to separate
 103 feature content and positional contributions. It is general and compatible with any attribution method.

104 Given feature $x \in \mathcal{X}$ and position $p \in \mathcal{P}$, the framework outputs

$$\alpha = g(f, x, p) \in \mathbb{R}^{2d}, \quad (2)$$

105 which decomposes as

$$\alpha = (\alpha^{(\text{feature})}, \alpha^{(\text{position})}), \quad \alpha^{(\text{feature})} \in \mathbb{R}^d, \alpha^{(\text{position})} \in \mathbb{R}^d. \quad (3)$$

106 As shown in Equation (3), our framework explainer g requires f, x, p as input, meaning we are
 107 also using p to show the positional influence for the prediction. Figure 1 shows the example of
 108 highlighting $\alpha^{(\text{feature})}$ and $\alpha^{(\text{position})}$ for one example across timestamps. The interpretation of $\alpha^{(\text{feature})}$
 109 and $\alpha^{(\text{position})}$ are as follows:

- 110 1. **Feature Content Attribution** ($\alpha_i^{(\text{feature})}$): Measures the effect of perturbing x_i while keeping
 111 p_i fixed. Answers: *How important is the feature content itself, given its location?*
- 112 2. **Absolute Position Attribution** ($\alpha_i^{(\text{position})}$): Measures the intrinsic value of p_i by comparing
 113 contributions of x_i at its original versus random positions. Answers: *How important is this
 114 location, independent of the feature content?*

Table 1: Performance of GPT2 and Mamba on the MC-MED and Physionet datasets. The models achieve sufficiently high predictive performance on sepsis prediction tasks, making them suitable for subsequent analysis and explanation.

Dataset	Finetuned Model	Accuracy	F1	AUC	AUPRC
PhysioNet [Reyna et al., 2020]	GPT-2 [Radford et al., 2019]	0.8680	0.2048	0.7069	0.1802
	Mamba [Gu and Dao, 2024]	0.8930	0.0531	0.3509	0.0403
MC-MED [Kansal et al., 2025]	GPT-2 [Radford et al., 2019]	0.9490	0.1053	0.3536	0.0900
	Mamba [Gu and Dao, 2024]	0.8940	0.0536	0.3743	0.0443

115 **Positional-LIME as an Example.** To illustrate, consider LIME [Ribeiro et al., 2016]. Standard
 116 LIME generates perturbed samples

$$z = m \odot x \in \mathbb{R}^d, \quad m_i \sim \text{Bernoulli}(0.5), \quad (4)$$

117 where $m_i = 0$ zeros out x_i and $m_i = 1$ retains it. LIME then fits a weighted linear model

$$\alpha = g(f, x) = w \in \mathbb{R}^d, \quad (5)$$

118 so that each α_i reflects the local effect of x_i on $f(x)$.

119 In **Positional-LIME**, positions are treated as additional features. To avoid out-of-distribution issues
 120 from zeroing positional embeddings, we instead randomize them:

$$z = m \odot (x, p) \in \mathbb{R}^{2d}, \quad m_i \sim \text{Bernoulli}(0.5), \quad (6)$$

121 where $m_i = 0$ indicates that the feature x_i is masked and the corresponding position p_i is replaced
 122 with random positional embedding.

123 The resulting attributions

$$\alpha = g(f, x, p) = w \in \mathbb{R}^{2d} \quad (7)$$

124 can then be separated into feature and positional contributions:

$$\alpha = (\alpha^{(\text{feature})}, \alpha^{(\text{position})}), \quad \alpha^{(\text{feature})} \in \mathbb{R}^d, \alpha^{(\text{position})} \in \mathbb{R}^d. \quad (8)$$

125 **Generalization to Other Explainers.** More generally, this framework extends to any attribution
 126 method (e.g., SHAP [Lundberg and Lee, 2017], Integrated Gradients [Sundararajan et al., 2017],
 127 FullGrad [Srinivas and Fleuret, 2019], MFABA [Zhu et al., 2024]). By computing $\alpha^{(\text{feature})}$ and
 128 $\alpha^{(\text{position})}$ separately, we separate feature content and positional contributions, providing a more
 129 fine-grained understanding of model predictions.

130 4 Experiments

131 We evaluated GPT-2 small (124M) [Radford et al., 2019] and Mamba-130M [Gu and Dao, 2024] on
 132 sepsis prediction tasks using the MC-MED [Kansal et al., 2025] and Physionet [Reyna et al., 2020]
 133 datasets. For each model, we used pre-trained, fine-tuned checkpoints provided by the CareBench
 134 benchmark [Choi et al., 2025] and assessed performance directly on the corresponding test sets.

135 Physionet is a widely used publicly available sepsis dataset containing only tabular EHR data, whereas
 136 MC-MED provides more comprehensive information, including ECG and respiratory waveforms,
 137 ventilator settings, medications, and per-minute vitals. Following the CareBench evaluation pro-
 138 tocol [Choi et al., 2025], we adopted the benchmark’s sepsis labeling criteria and cohort selection
 139 methodology, ensuring consistent preprocessing and evaluation conditions across both models and
 140 datasets.

141 Table 1 summarizes model performance across four metrics: Accuracy (Acc), F1-score (F1), Area
 142 Under the Receiver Operating Characteristic curve (AUC), and Area Under the Precision-Recall
 143 Curve (AUPRC). Both models achieved strong predictive performance, establishing them as suitable
 144 candidates for subsequent explanation analyses.

Table 2: Insertion and deletion test results on the MC-MED and PhysioNet datasets using Positional-LIME for finetuned GPT-2 and Mamba models. The table reports Area Under the Curve (AUC) averaged over all examples. Using the feature component of Positional-LIME consistently outperforms feature-only attributions, and using the positional component consistently outperforms position-only attributions. This demonstrates that separating attributions into feature and positional components with our framework produces more faithful explanations.

(a) Insertion AUC (higher is better).

Dataset	Model	Feature-only	Position-only	PE-Feature	PE-Position	PE-Full	Random
PhysioNet	GPT-2	0.354	0.323	0.419	0.396	0.465	0.214
	Mamba	0.347	0.331	0.392	0.401	0.454	0.213
MC-MED	GPT-2	0.313	0.301	0.381	0.392	0.434	0.192
	Mamba	0.319	0.311	0.393	0.403	0.442	0.201

(b) Deletion AUC (lower is better).

Dataset	Model	Feature-only	Position-only	PE-Feature	PE-Position	PE-Full	Random
PhysioNet	GPT-2	0.020	0.016	0.008	0.007	0.002	0.110
	Mamba	0.021	0.019	0.011	0.007	0.001	0.102
MC-MED	GPT-2	0.007	0.032	0.006	0.011	0.005	0.226
	Mamba	0.072	0.113	0.066	0.053	0.045	0.199

145 4.1 Faithfulness Test

146 We examine whether decomposing attributions into feature and positional components using our
 147 *Positional Explanation* framework improves explanation faithfulness in clinical settings. This decom-
 148 position enables differentiation between patients whose high risk stems from chronically abnormal
 149 lab values and those whose risk arises from sudden, recent changes, supporting more targeted clinical
 150 review.

151 To evaluate faithfulness, we conduct insertion and deletion tests and report average AUC scores. We
 152 compare six conditions: feature-only baseline, position-only baseline, PE-Feature (feature component
 153 from *Positional Explanation*), PE-Position (positional component from *Positional Explanation*),
 154 PE-Combined (both components from *Positional Explanation*), and a random baseline. Detailed
 155 descriptions of each approach are provided in Appendix B.

156 **Across Datasets and Models** Across datasets and models (further details on datasets and model
 157 setups are provided in Appendix A), PE-Feature consistently achieves higher insertion scores and
 158 lower deletion scores than Feature-only, while PE-Position achieves higher insertion and lower
 159 deletion scores than Position-only. Full insertion results are reported in Table 4a, and full deletion
 160 scores are reported in Table 4b. This demonstrates that separating feature and positional components
 161 results in more faithful attributions.

162 **Across Explainability Methods** We evaluate faithfulness across several explainability methods
 163 on the MC-MED dataset with GPT-2, comparing Feature-only (traditional perturbation), Position-
 164 only (position perturbation), PE-Feature (feature component of our *Positional Explanation*), and
 165 PE-Position (positional component of our *Positional Explanation*). The methods considered include
 166 LIME [Ribeiro et al., 2016], SHAP [Lundberg and Lee, 2017], Integrated Gradients [Sundararajan
 167 et al., 2017], FullGrad [Srinivas and Fleuret, 2019], and MFABA [Zhu et al., 2024] (see Appendix A.3
 168 for details).

169 Although we show results here only for PhysioNet with GPT-2, the trend is consistent across all
 170 methods: PE-Feature achieves higher insertion and lower deletion scores than Feature-only, and PE-
 171 Position achieves higher insertion and lower deletion scores than Position-only. These results indicate
 172 that separating feature and positional components consistently produces more faithful explanations,
 173 independent of the underlying attribution method.

Table 3: Faithfulness comparison across explainability methods on PhysioNet using GPT-2. We report AUC for both insertion and deletion tests. Across methods, PE-Feature consistently outperforms Feature-only and PE-Position outperforms Position-only, showing that separating attributions into feature and positional components using our framework leads to more faithful explanations.

(a) Insertion AUC (higher is better).

Explanation Method	Feature-only	Position-only	PE-Feature	PE-Position
LIME [Ribeiro et al., 2016]	0.354	0.323	0.419	0.396
SHAP [Lundberg and Lee, 2017]	0.342	0.337	0.403	0.401
Integrated Gradients [Sundararajan et al., 2017]	0.361	0.346	0.427	0.412
FullGrad [Srinivas and Fleuret, 2019]	0.336	0.314	0.384	0.393
MFABA [Zhu et al., 2024]	0.351	0.325	0.417	0.402

(b) Deletion AUC (lower is better).

Explanation Method	Feature-only	Position-only	PE-Feature	PE-Position
LIME [Ribeiro et al., 2016]	0.020	0.016	0.008	0.007
SHAP [Lundberg and Lee, 2017]	0.019	0.018	0.007	0.008
Integrated Gradients [Sundararajan et al., 2017]	0.019	0.021	0.009	0.011
FullGrad [Srinivas and Fleuret, 2019]	0.017	0.019	0.010	0.010
MFABA [Zhu et al., 2024]	0.018	0.015	0.007	0.006

174 4.2 Independence Test

175 We assessed whether feature ($\alpha^{(\text{feature})}$) and positional ($\alpha^{(\text{position})}$) attributions are linearly related per
 176 measurement using the Pearson correlation coefficient. A high correlation magnitude indicates a
 177 strong linear relationship, whereas a low magnitude suggests independence. Statistical significance
 178 was evaluated using p -values, representing the likelihood that an observed correlation occurred by
 179 chance (see Appendix C.1.1 for computation details).

180 Figure 2 shows the distribution of absolute correlation values across measurements. The results
 181 indicate variability in temporal dependence: some measurements strongly depend on time, while
 182 others are largely independent.

183 Examples of temporal correlation analysis of measurements in the MC-MED dataset using GPT-2
 184 with Position-LIME:

185 **High temporal correlation:** LABPTT, GLOBULIN, WAM DIFTYP, TEMP

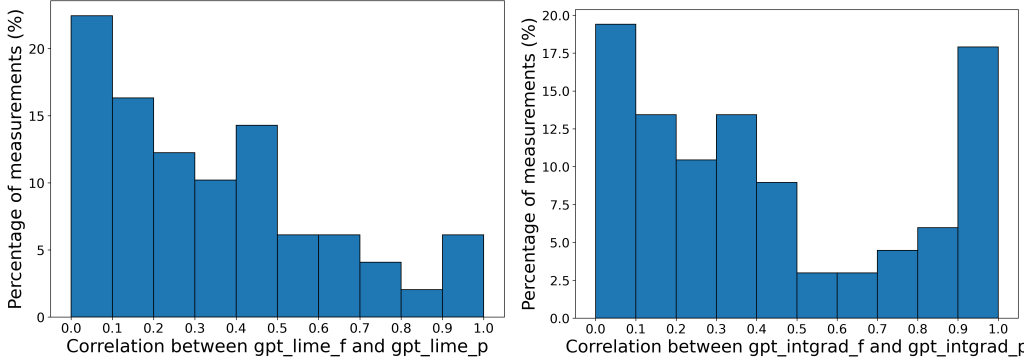
186 **Low temporal correlation:** AGE, RACE, AST (SGOT), PLATELET COUNT (PLT)

187 These findings suggest that static variables (e.g., demographics, baseline labs) are generally position-
 188 independent, whereas dynamic variables (e.g., coagulation tests, temperature) exhibit strong temporal
 189 dependence. Full correlation values and p -values are reported in Appendix C.1.2.

190 To validate our hypothesis that separating attribution into feature and positional components is helps
 191 identifying true temporal dependencies, we conduct an evaluation using a Large Language Model
 192 (LLM) as a proxy for ground-truth verification. We compare two methods for measuring temporal
 193 correlations, with results presented in Figure 3.

194 The baseline uses correlation between feature-only and position-only attribution. We compare it
 195 to correlation between PE-Feature and PE-Position using our Positional Explanation framework.
 196 For evaluation, we group feature-position pairs into three bins based on their computed correlation
 197 scores: high correlation (correlation > 0.7), moderate correlation ($0.3 < \text{correlation} \leq 0.7$), and low
 198 correlation ($\text{correlation} \leq 0.3$). Within each bin, we measure the LLM verification accuracy to assess
 199 how well our correlation scores align with LLM-verified temporal dependencies. The results show
 200 that our PE-based attribution consistently achieves higher verification rates across all correlation bins,
 201 demonstrating that separating the score improves the identification of features with genuine temporal
 202 effects and confirming the effectiveness of our method in detecting temporal correlations.

203 We also show qualitative result of what the LLM output for such correlation in Appendix C



(a) Histogram of Correlations for measurements ap-predding more than 5 times using LIME (b) Histogram of Correlations for measurements ap-predding more than 5 times using Integrated Gradients

Figure 2: Histogram of absolute correlation between feature (f) and positional (p) attribution per measurement. From these two histograms of LIME and Integrated Gradients, we observe that some measurements are inherently time-correlated while others are not, and these patterns differ across explanation methods.

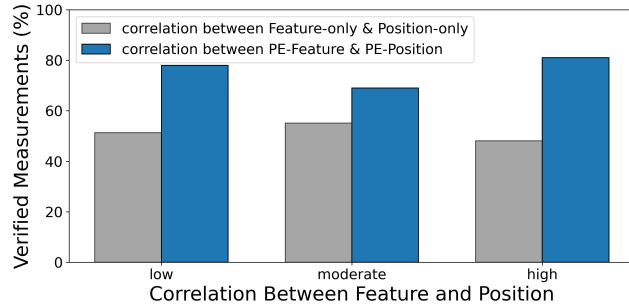


Figure 3: LLM verification accuracy for temporal correlation detection across different correlation bins. Our Positional Explanation (PE) framework, which correlates PE-Feature and PE-Position scores after separation, consistently outperforms the baseline method that directly correlates feature-only and position-only attributions. Higher verification accuracy across all bins demonstrates that decomposing attribution signals better identifies measurements with genuine temporal dependencies, helping clinicians distinguish between time-correlated and time-independent measurements.

204 4.3 Relevance Test

205 To evaluate the quality of feature attributions, we conducted a systematic comparison between traditional
206 feature-only explanations and our Positional Explanation framework using LLM verification.
207 We analyzed feature importance scores across clinical measurements to assess which method more
208 accurately identifies clinically relevant features independent of temporal context.

209 For quantitative evaluation, we computed average feature importance scores across the entire dataset
210 and organized features into three bins based on their attribution scores: high influence, moderate in-
211 fluence, and low influence. The top 10 most influential measurements identified using our framework
212 include: INFLUENZA B, NUR1373, ALBUMIN, POC16, KETONE: URINE (UA), SARS-COV-2
213 RNA, MYCOPLASMA PNEUMONIAE, POC:KETONE, POC:GLUCOSE BY METER, MAGNESIUM.

214 Figure 4 presents the LLM verification results comparing feature-only attributions (original expla-
215 nation method that perturbs only features) against PE-Feature scores from our Positional Explanation
216 framework (which perturbs both features and positions before extracting the feature component). The
217 results demonstrate that our PE-Feature approach consistently achieves higher LLM verification accu-
218 racy across all influence bins. This superior performance confirms that disentangling positional and
219 feature effects produces more clinically meaningful feature attributions, enabling better identification
220 of truly relevant measurements for clinical decision-making.

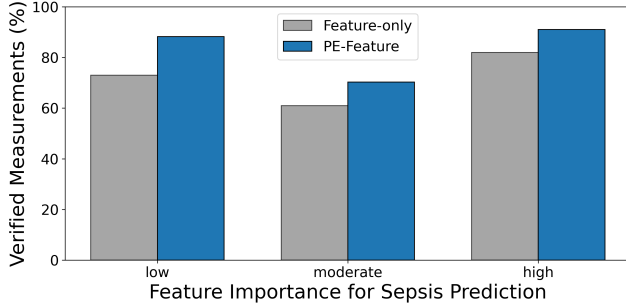


Figure 4: LLM verification accuracy for feature attribution methods. Our PE-Feature scores from the Positional Explanation framework achieve higher LLM verification accuracy compared to feature-only attributions, demonstrating improved feature attribution quality through separation.

221 We also show qualitative result of what the LLM output for such feature was in Appendix D

222 5 Conclusion

223 We introduced the *Positional Explanation* framework, which separates standard feature attributions
 224 into *feature content* and *position* effects, enabling explanations that distinguish *what* drives a model’s
 225 prediction from *when* it is clinically significant. Applied to Mamba and GPT-2 models finetuned
 226 for sepsis prediction on PhysioNet and MC-MED datasets, our approach provides more faithful,
 227 temporally aware explanations than existing explanation methods, and identifies clinically relevant,
 228 time-dependent biomarkers that are otherwise overlooked. Importantly, Positional Explanation is
 229 model- and method-agnostic and can be applied to any feature attribution framework for any types of
 230 data including image, text, and time-series.

231 While these results are promising, broader clinical validation is necessary. Current evaluation
 232 relies primarily on LLM-based models. We will engage multiple clinicians specialized in sepsis to
 233 evaluate real-world interpretability, trust, and utility. To demonstrate generality, we plan to extend the
 234 framework to new models, develop scalable metrics for temporal effects, and integrate it into clinical
 235 decision support systems for timely, actionable alerts.

236 Overall, Positional Explanation provides a general, flexible framework for temporally aware explain-
 237 ability in clinical predictive modeling, bridging the gap between accurate prediction and actionable,
 238 time-sensitive insight.

239 References

240 Roy Adams, Kevin E. Henry, Anoop Sridharan, Heather Soleimani, Karandeep A. Zell, Chuan
 241 S. L. Tan, Jenna N. Wiens, Craig E. V. Barton, and Karandeep A. Singh. Prospective, multi-site
 242 study of a deep learning model for early detection of sepsis. *Nature Medicine*, 28(8):1649–1654,
 243 2022. doi: 10.1038/s41591-022-01894-0.

244 João Bento, Pedro Saleiro, Pedro Bizarro, and Mário A T Oliveira. Timeshap: Explaining recurrent
 245 models through time. In *2021 International Conference on Data Mining Workshops (ICDMW)*,
 246 pages 336–345. IEEE, 2021.

247 Sherali Bomrah, Mohy Uddin, Umashankar Upadhyay, Jyoti Priya, Eshita Dhar, Shih-Chang Hsu,
 248 and Shabir Syed-Abdul. A scoping review of machine learning for sepsis prediction- feature
 249 engineering strategies and model performance: a step towards explainability. *Critical Care*, 28:
 250 180, 2024.

251 Seewon Choi, Mayank Keoliya, Rajeev Alur, Mayur Naik, and Eric Wong. Carebench: Stable
 252 prediction of adverse events in medical time-series data, 2025.

253 Jonathan Crabbé and Mihaela van der Schaar. Explaining time series predictions with dy-
 254 namic masks. In H. Larochelle, M. Ranzato, R. Hadsell, M. F. Balcan, and H. Lin, edi-

255 tors, *Advances in Neural Information Processing Systems*, volume 33, pages 1236–1247. Cur-
256 ran Associates, Inc., 2020. URL <https://proceedings.neurips.cc/paper/2020/file/084a0c2053618953a0a65261394338d3-Paper.pdf>.

258 Finale Doshi-Velez and Been Kim. Towards a rigorous science of interpretable machine learning,
259 2017.

260 Yash Goyal, Been Kim Wu, and Joachim Ernst. Counterfactual explanations for time-series mod-
261 els. In M. Ranzato, A. Beygelzimer, Y. Dauphin, P.S. Liang, and J. Wortman Vaughan, edi-
262 tors, *Advances in Neural Information Processing Systems*, volume 34, pages 1496–1508. Cur-
263 ran Associates, Inc., 2021. URL <https://proceedings.neurips.cc/paper/2021/file/0e64a7b12e34720385965191838b08cd-Paper.pdf>.

265 Albert Gu and Tri Dao. Mamba: Linear-time sequence modeling with selective state spaces, 2024.
266 URL <https://arxiv.org/abs/2312.00752>.

267 Aaqib Ismail and Stephan Günnemann. Benchmarking deep learning interpretability in time series
268 predictions. *Advances in Neural Information Processing Systems*, 34:23605–23618, 2021.

269 Sarthak Jain and Byron C. Wallace. Attention is not explanation, 2019. URL <https://arxiv.org/abs/1902.10186>.

271 Anshul Kansal, Eric Chen, Billy T. Jin, et al. MC-MED, multimodal clinical monitoring in the
272 emergency department. *Scientific Data*, 12:1094, 2025. doi: 10.1038/s41597-025-05419-5.

273 Simon Meyer Lauritsen, Martin Kristensen, Mads Vincent Olsen, and Michael Stig Larsen. Explain-
274 able artificial intelligence model to predict acute critical illness from electronic health records.
275 *Nature Communications*, 11(1):3852, 2020.

276 Nelson F. Liu, Kevin Lin, John Hewitt, Ashwin Paranjape, Michele Bevilacqua, Fabio Petroni, and
277 Percy Liang. Lost in the middle: How language models use long contexts. *Transactions of the
278 Association for Computational Linguistics*, 12:157–173, 2024. doi: 10.1162/tacl_a_00638.

279 Scott M. Lundberg and Su-In Lee. A unified approach to interpreting model predictions. In
280 *Proceedings of the 31st International Conference on Neural Information Processing Systems
281 (NIPS)*, pages 4768–4777, 2017.

282 Alec Radford, Jeffrey Wu, Rewon Child, David Luan, Dario Amodei, and Ilya Sutskever. Language
283 models are unsupervised multitask learners. 2019.

284 Matthew A. Reyna, Christopher S. Josef, Russell Jeter, Supreeth P. Shashikumar, M. Brandon
285 Westover, Shamim Nemati, Gari D. Clifford, and Ashish Sharma. Early prediction of sepsis from
286 clinical data: the physionet/computing in cardiology challenge 2019. *Critical Care Medicine*, 48
287 (2):210–217, 2020.

288 Marco Tulio Ribeiro, Sameer Singh, and Carlos Guestrin. "Why Should I Trust You?": Explaining the
289 Predictions of Any Classifier. In *Proceedings of the 22nd ACM SIGKDD International Conference
290 on Knowledge Discovery and Data Mining*, pages 1135–1144, 2016.

291 Christopher W Seymour, Vincent X Liu, Theodore J Iwashyna, Frank M Brunkhorst, Thomas D
292 Rea, André Scherag, Gordon Rubenfeld, Jeremy M Kahn, Manu Shankar-Hari, Mervyn Singer,
293 Clifford S Deutschman, Gabriel J Escobar, and Derek C Angus. Assessment of clinical criteria
294 for sepsis: For the third international consensus definitions for sepsis and septic shock (sepsis-3).
295 *JAMA*, 315(8):762–774, 2016. doi: 10.1001/jama.2016.0288.

296 Supreeth P. Shashikumar, Gabriel Wardi, Atul Malhotra, and Shamim Nemati. Artificial intelligence
297 sepsis prediction algorithm learns to say "i don't know". *npj Digital Medicine*, 4(1):134, 2021.
298 doi: 10.1038/s41746-021-00504-6.

299 Benjamin Shickel, Patrick J Tighe, Azra Bihorac, and Parisa Rashidi. Deep ehr: A survey of recent
300 advances in deep learning for electronic health records. In *IEEE journal of biomedical and health
301 informatics*, volume 22, pages 1589–1604. IEEE, 2017.

302 Suraj Srinivas and François Fleuret. Full-gradient representation for neural network visualization. In
303 *Advances in Neural Information Processing Systems* 32, 2019.

304 Mukund Sundararajan, Ankur Taly, and Qiqi Yan. Axiomatic attribution for deep networks. In
305 *Proceedings of the 34th International Conference on Machine Learning (ICML)*, pages 3319–3328,
306 2017.

307 Sana Tonekaboni, Shalmali Joshi, Michael D McCradden, and Anna Goldenberg. What clinicians
308 want: a survey of explainable ai needs for clinical decision support. In *Proceedings of the 2019*
309 *CHI Conference on Human Factors in Computing Systems*, pages 1–13, 2019.

310 Eric J Topol. High-performance medicine: the convergence of human and artificial intelligence.
311 *Nature medicine*, 25(1):44–56, 2019.

312 Ashish Vaswani, Noam Shazeer, Niki Parmar, Jakob Uszkoreit, Llion Jones, Aidan N Gomez, Łukasz
313 Kaiser, and Illia Polosukhin. Attention is all you need. In *Advances in neural information*
314 *processing systems*, pages 5998–6008, 2017.

315 Peiyi Wang, Lei Li, Liang Chen, Zefan Cai, Dawei Zhu, Binghuai Lin, Yunbo Cao, Lingpeng Kong,
316 Qi Liu, Tianyu Liu, and Zhifang Sui. Large language models are not fair evaluators. In Lun-
317 Wei Ku, Andre Martins, and Vivek Srikumar, editors, *Proceedings of the 62nd Annual Meeting*
318 *of the Association for Computational Linguistics (Volume 1: Long Papers)*, pages 9440–9450.
319 Association for Computational Linguistics, 2024. doi: 10.18653/v1/2024.acl-long.511.

320 Andrew Wong, Erkin Otles, John P. Donnelly, Andrew Krumm, J. Michael McCullough, Olivia
321 DeTroyer-Cooley, Jennifer Pestreue, M. Elizabeth Phillips, Justin Konye, Patrick J. Schulte, Mihir
322 A. Kora, Dmitriy A. Dligach, and Majid Afshar. External validation of a widely implemented
323 commercial sepsis prediction model in hospitalized patients. *JAMA Internal Medicine*, 181(8):
324 1065–1070, 2021. doi: 10.1001/jamainternmed.2021.2626.

325 Kuo-Ching Yuan, Lung-Wen Tsai, Ko-Han Lee, Yi-Wei Cheng, Shou-Chieh Hsu, Yu-Sheng Lo, and
326 Ray-Jade Chen. The development an artificial intelligence algorithm for early sepsis diagnosis in
327 the intensive care unit. *International Journal of Medical Informatics*, 141:104176, 2020.

328 Jia-Liang Zhu, Shi-Qi Yuan, Tao Huang, Lu-Ming Zhang, Xiao-Mei Xu, Hai-Yan Yin, Jian-Rui Wei,
329 and Jun Lyu. Influence of systolic blood pressure trajectory on in-hospital mortality in patients
330 with sepsis. *BMC Infectious Diseases*, 23(1):90, 2023.

331 Zhiyu Zhu, Huaming Chen, Jiayu Zhang, Xinyi Wang, Zhibo Jin, Minhui Xue, Dongxiao Zhu, and
332 Kim-Kwang Raymond Choo. Mfaba: A more faithful and accelerated boundary-based attribution
333 method for deep neural networks. *Proceedings of the AAAI Conference on Artificial Intelligence*,
334 38(15):17228–17236, 2024. doi: 10.1609/aaai.v38i15.29669.

335 A Experimental Setup

336 A.1 Dataset Description

337 A.1.1 Datasets

338 We utilize sepsis prediction datasets curated by CAREBench [Choi et al., 2025], which processes two
339 publicly available datasets: PhysioNet 2019 [Reyna et al., 2020] and MC-MED [Kansal et al., 2025].

340 **PhysioNet 2019** comprises over 40,000 ICU patients with up to 40 clinical variables recorded hourly,
341 totaling 2.5 million hourly time windows. The dataset includes vital signs, laboratory values, and
342 demographics in tabular format without physiological waveforms.

343 **MC-MED** contains 118,385 emergency department visits from 70,545 unique patients (2020–2022).
344 This dataset uniquely combines minute-level vital signs and continuous physiological waveforms
345 (ECG, photoplethysmogram, respiration) with comprehensive clinical data including demographics,
346 medical histories, medications, and laboratory results.

347 **A.1.2 Sepsis Prediction Task Curation**

348 CAREBench adapted the curation methodology to each dataset’s clinical setting and available data.

349 **PhysioNet 2019:** Sepsis labels were pre-defined using Sepsis-3 criteria, requiring both clinical
350 suspicion of infection (blood culture or IV antibiotic orders) and a two-point SOFA score change.

351 **MC-MED:** CAREBench implemented a two-stage process:

352 1. **At-Risk Cohort Selection** – Patients meeting all criteria:

- 353 • Admission source of ED
- 354 • Temperature $< 36^{\circ}\text{C}$ or $> 38.5^{\circ}\text{C}$ within 24 hours of admission (Temp_time)
- 355 • At least one of the following within 24 hours of admission:
 - 356 ○ WBC Count $> 12K$ or $< 4K/\mu\text{L}$ (WBC_time)
 - 357 ○ HR > 90 bpm (HR_time)
 - 358 ○ RR > 20 (RR_time)
- 359 • At least 1 of the WBC_time, HR_time, RR_time within 12 hours of Temp_time
- 360 • No intravenous antibiotic at or before the time of the first criteria met

361 2. **Sepsis Labeling** – Adapted Sepsis-3 definition for ED settings with $h = 1.5$ hour prediction
362 horizon. Positive labels assigned when emergency SOFA (eSOFA) criteria met:

- 363 • Presumed serious infection:
 - 364 ○ Blood culture obtained (regardless of the results)
 - 365 ○ ≥ 4 QADs starting within ± 2 days of blood_culture_day
- 366 • Any 1 of below within ± 2 days of blood_culture_day (acute organ dysfunction):
 - 367 ○ Vasopressor initiation
 - 368 ○ Initiation of mechanical ventilation
 - 369 ○ Doubling in serum creatinine level or decrease by $\geq 50\%$ of eGFR (excluding patients
370 with end-stage kidney disease [585.6])
 - 371 ○ Total bilirubin level $\geq 2.0\text{mg/dL}$ and doubling
 - 372 ○ Platelet count $< 100 \text{ cells}/\mu\text{L}$ and $\geq 50\%$ decline from baseline (excluding baseline $<$
373 $100 \text{ cells}/\mu\text{L}$)
 - 374 ○ Serum lactate $\geq 2.0 \text{ mmol/L}$

375 **A.2 Model Description**

376 We employed GPT-2 (124M parameters) [Radford et al., 2019] and Mamba-130M [Gu and Dao,
377 2024], pre-trained language models fine-tuned for sepsis prediction using the CAREBench-curated
378 datasets.

379 **A.2.1 Model Architectures**

380 **GPT-2 Small:** A 124M parameter decoder-only transformer with 12 layers, 768 hidden dimensions,
381 and 12 attention heads. Its autoregressive architecture with causal self-attention naturally captures
382 temporal dependencies in patient trajectories, leveraging pre-trained sequential representations for
383 modeling physiological progression patterns.

384 **Mamba-130M:** A 130M parameter state-space model addressing transformer limitations in long-
385 sequence processing. Its selective state-space mechanism achieves linear complexity with sequence
386 length, enabling efficient processing of extended patient histories. The architecture’s continuous-time
387 formulation aligns naturally with physiological processes, offering advantageous inductive biases for
388 modeling sepsis dynamics.

389 **A.2.2 Training Configuration**

390 Following CAREBench methodology:

- 391 • **Custom Tokenization:** Dataset-specific tokenizers handle hospital-specific medical codes and
392 limited vocabulary
- 393 • **Training Duration:** 100 epochs ensuring convergence on limited medical data

394 • **Hyperparameter Selection:** Learning rate $\in \{1 \times 10^{-5}, 5 \times 10^{-5}, 1 \times 10^{-4}\}$ via validation
395 performance

396 This configuration enables effective adaptation from general language understanding to domain-
397 specific temporal patterns and medical terminology in sepsis prediction.

398 **A.3 Explanation Methods**

399 This section briefly describes the explanation methods employed in conjunction with our Positional
400 Explanation approach.

401 • **LIME (Local Interpretable Model-agnostic Explanations)** [Ribeiro et al., 2016] generates
402 local explanations for individual predictions by fitting an interpretable surrogate model (typically
403 linear) within the neighborhood of the target instance. The method creates perturbations around
404 the input sample and trains the surrogate model on these variations, with samples weighted by
405 their proximity to the original instance.

406 • **SHAP (SHapley Additive exPlanations)** [Lundberg and Lee, 2017] computes feature import-
407 tance scores based on cooperative game theory principles. Each feature receives an attribution
408 value representing its marginal contribution to the prediction relative to a baseline, with the
409 property that all attribution values sum to the difference between the model’s output and the
410 baseline prediction.

411 • **Integrated Gradients (IntGrad)** [Sundararajan et al., 2017] computes feature attributions by
412 integrating gradients along a linear path from a baseline input to the target input. This path
413 integral approach ensures satisfaction of fundamental attribution axioms, including sensitivity
414 and implementation invariance.

415 • **FullGrad** [Srinivas and Fleuret, 2019] extends standard gradient-based attribution by incorpo-
416 rating gradient information from all network layers. The method aggregates input gradients with
417 bias gradients across all intermediate representations, providing more comprehensive attribution
418 maps that capture multi-layer feature interactions.

419 • **MFABA (More Faithful and Accelerated Boundary-based Attribution)** [Zhu et al., 2024]
420 computes attributions by constructing paths from input samples to adversarial examples that
421 cross the model’s decision boundary. The method employs second-order Taylor approximations
422 to better model loss function changes during gradient ascent optimization.

423 **B Additional Faithfulness Test Results**

424 This section presents comprehensive results from our insertion and deletion experiments across all
425 experimental configurations. We systematically evaluate faithfulness across two datasets (PhysioNet
426 and MC-MED), two transformer architectures (GPT-2 and Mamba), and five explanation methods
427 (LIME, SHAP, Integrated Gradients, FullGrad, MFABA).

428 **B.1 Faithfulness Test Experimental Setup**

429 For each explanation method, we compare five attribution approaches:

430 • **Feature-only:** Traditional perturbation-based explanations
431 • **Position-only:** Positional explanation perturbing only position
432 • **PE-Feature:** Feature component of our *Positional Explanation* framework
433 • **PE-Position:** Position component of our *Positional Explanation* framework
434 • **PE-Full:** Both feature and position components of our *Positional Explanation* framework
435 • **Random:** Baseline for comparison

436 We employ two complementary faithfulness metrics: insertion tests (where higher AUC indicates
437 better faithfulness) and deletion tests (where lower AUC indicates better faithfulness).

438 **B.2 Key Findings**

439 The results demonstrate consistent improvements in explanation faithfulness when separating posi-
440 tional and feature components:

441 **Insertion Test Performance.** Our positional explanation components (PE-Feature and PE-Position)
442 consistently outperform their traditional counterparts (Feature-only and Position-only) across all
443 experimental configurations. PE-Feature achieves higher AUC scores than Feature-only, while
444 PE-Position surpasses Position-only, indicating more faithful identification of important features.

445 **Deletion Test Performance.** The superiority of our approach is further confirmed in deletion
446 tests, where PE-Feature consistently achieves lower AUC scores than Feature-only, and PE-Position
447 outperforms Position-only. Lower scores in deletion tests indicate that removing highly-attributed
448 features causes greater performance degradation, confirming these features are indeed more important
449 for model predictions.

450 **Cross-Architecture and Cross-Method Consistency.** The improvements hold across both GPT-
451 2 and Mamba architectures, as well as different explanation methods including gradient-based
452 attribution, attention-based explanations, and perturbation-based approaches, demonstrating the broad
453 generalizability of our positional explanation approach.

454 **B.3 Detailed Results**

455 Tables 4a and 4b present the complete faithfulness evaluation results across all experimental configu-
456 rations. The insertion test results demonstrate the ability of each method to identify truly important
457 features, while the deletion test results show how effectively each method identifies features whose
458 removal significantly impacts model performance. These comprehensive results validate our theoret-
459 ical framework and demonstrate the practical benefits of separating positional and feature attributions
460 in transformer explanations.

461 **C Additional Independence Test Results**

462 **C.1 Independence Test Analysis**

463 This section presents the complete results from our independence test analysis, expanding on the
464 verification scores reported in Section 4.2.

465 **C.1.1 Measurements**

466 The correlation was measured using the Pearson correlation coefficient:

$$r = \frac{\sum_{i=1}^n (\alpha_i^{(\text{feature})} - \bar{\alpha}^{(\text{feature})})(\alpha_i^{(\text{position})} - \bar{\alpha}^{(\text{position})})}{\sqrt{\sum_{i=1}^n (\alpha_i^{(\text{feature})} - \bar{\alpha}^{(\text{feature})})^2} \sqrt{\sum_{i=1}^n (\alpha_i^{(\text{position})} - \bar{\alpha}^{(\text{position})})^2}}, \quad (9)$$

467 where $r \in [-1, 1]$, $\bar{\alpha}^{(\text{feature})}$ is the mean feature attribution, and $\bar{\alpha}^{(\text{position})}$ is the mean positional
468 attribution. Values of r close to 1 or -1 indicate strong positive or negative correlation, while values
469 near 0 suggest little to no linear relationship.

470 To assess statistical significance, we tested the null hypothesis:

$$H_0 : r = 0 \quad (\text{feature and positional attributions are uncorrelated}).$$

471 The corresponding p -value quantifies the probability of observing a correlation at least as extreme as
472 the measured r under H_0 . At the $\alpha = 0.05$ significance level,

473 • If $p < 0.05$: we reject H_0 , concluding significant correlation.
474 • If $p \geq 0.05$: we fail to reject H_0 , finding no clear evidence of correlation.

475 **C.1.2 Temporal Correlation Patterns**

476 Our analysis identified distinct patterns in temporal correlation across different medical measurements:

477 **Examples of independent features** (low correlation, high p -value) using Positional-LIME on the
478 MC-MED dataset with GPT-2 included:

Table 4: Our Positional Explanation (PE) framework consistently outperforms traditional attribution methods. PE-Feature and PE-Position achieve higher insertion AUC and lower deletion AUC than their Feature-only and Position-only counterparts, confirming more faithful identification of important features. The improvements hold across both GPT-2 and Mamba architectures and multiple explanation methods. PE = Positional Explanation, Feat = Feature, Pos = Position.

(a) Insertion test results (AUC). Higher values indicate more faithful performance.

Dataset	Model	Explanation	Feat-only	Pos-only	PE-Feat	PE-Pos	PE-Full	Random
PhysioNet	GPT-2	LIME	0.354	0.323	0.419	0.396	0.465	0.214
		SHAP	0.342	0.337	0.403	0.401	0.452	0.209
		IntGrad	0.361	0.346	0.427	0.412	0.478	0.221
		FullGrad	0.336	0.314	0.384	0.393	0.443	0.215
		MFABA	0.351	0.325	0.417	0.402	0.461	0.208
	Mamba	LIME	0.347	0.331	0.392	0.401	0.454	0.213
		SHAP	0.352	0.323	0.415	0.395	0.463	0.207
		IntGrad	0.364	0.348	0.431	0.416	0.472	0.226
		FullGrad	0.338	0.312	0.393	0.382	0.445	0.218
		MFABA	0.353	0.334	0.422	0.404	0.460	0.202
MC-MED	GPT-2	LIME	0.313	0.301	0.381	0.392	0.434	0.192
		SHAP	0.321	0.314	0.392	0.403	0.446	0.207
		IntGrad	0.332	0.322	0.413	0.421	0.461	0.215
		FullGrad	0.303	0.296	0.375	0.384	0.421	0.194
		MFABA	0.324	0.312	0.401	0.395	0.452	0.203
	Mamba	LIME	0.319	0.311	0.393	0.403	0.442	0.201
		SHAP	0.331	0.322	0.414	0.411	0.451	0.214
		IntGrad	0.339	0.336	0.421	0.432	0.463	0.223
		FullGrad	0.312	0.303	0.382	0.391	0.433	0.208
		MFABA	0.330	0.321	0.412	0.410	0.450	0.212

(b) Deletion test results (AUC). Lower values indicate more faithful performance.

Dataset	Model	Explanation	Feat-only	Pos-only	PE-Feat	PE-Pos	PE-Full	Random
PhysioNet	GPT-2	LIME	0.020	0.016	0.008	0.007	0.002	0.110
		SHAP	0.019	0.018	0.007	0.008	0.003	0.102
		IntGrad	0.019	0.021	0.009	0.011	0.005	0.112
		FullGrad	0.017	0.019	0.010	0.010	0.004	0.111
		MFABA	0.018	0.015	0.007	0.006	0.002	0.109
	Mamba	LIME	0.021	0.019	0.011	0.007	0.001	0.102
		SHAP	0.021	0.018	0.012	0.007	0.002	0.103
		IntGrad	0.011	0.011	0.008	0.009	0.003	0.111
		FullGrad	0.010	0.012	0.007	0.008	0.001	0.113
		MFABA	0.020	0.017	0.010	0.006	0.001	0.100
MC-MED	GPT-2	LIME	0.007	0.032	0.006	0.011	0.005	0.226
		SHAP	0.011	0.024	0.010	0.013	0.006	0.228
		IntGrad	0.053	0.103	0.037	0.077	0.035	0.218
		FullGrad	0.049	0.098	0.036	0.064	0.032	0.220
		MFABA	0.022	0.030	0.014	0.012	0.015	0.225
	Mamba	LIME	0.072	0.113	0.066	0.053	0.045	0.199
		SHAP	0.085	0.116	0.058	0.056	0.046	0.201
		IntGrad	0.089	0.102	0.047	0.057	0.033	0.204
		FullGrad	0.086	0.098	0.046	0.055	0.031	0.206
		MFABA	0.071	0.111	0.065	0.052	0.044	0.200

479 • AGE: correlation = 0.0244, $p = 0.9020$
480 • RACE: correlation = -0.0330, $p = 0.8675$
481 • AST (SGOT): correlation = -0.0082, $p = 0.9668$
482 • PLATELET COUNT (PLT): correlation = 0.0301, $p = 0.8888$

Gemini 2.5 pro

High Time-Correlated Features (Progression Markers): These features track continuous underlying sepsis pathophysiology.

- **LABPTT (Partial Thromboplastin Time):** PTT prolongs progressively in sepsis due to coagulation abnormalities (DIC), reflecting worsening condition over time.
- **GLOBULIN:** Reflects immune activity; levels gradually rise with ongoing infection, indicating systemic immune response.
- **WAM DIFTYP:** Likely tracks shifts in immune cell populations, reflecting the bone marrow's response to infection.

Low Time-Correlated Features (Condition Markers): These features reflect snapshots of patient state or specific events rather than continuous trends.

- **EKG5:** Captures heart electrical activity at an instant; changes are rapid, non-linear.
- **AST (SGOT) & PLT:** Organ damage markers; can remain stable and drop suddenly.
- **LYMPHOCYTE %:** Fluctuates relative to other WBCs; no consistent linear trend.

Figure 5: Feature temporal correlation analysis for sepsis prediction using Gemini 2.5 Pro. Features are categorized into High, Moderate, and Low time-correlated groups, reflecting progression markers, intermediate trends, and condition markers, respectively, as verified using the prompt shown in fig. 9.

483 **Examples of independent features** (low correlation, high p -value) using Positional-LIME on the
484 MC-MED dataset with GPT-2 included:

485 • LABPTT: correlation = 0.9080, $p = 1.11e-04$
486 • GLOBULIN: correlation = 0.9061, $p = 3.90e-05$
487 • WAM DIFTYP: correlation = 0.8447, $p = 2.15e-03$
488 • TEMP: correlation = 0.6659, $p = 3.55e-02$

489 These findings suggest that certain static variables (e.g., demographics, baseline labs) remain position-
490 independent, while dynamic variables (e.g., coagulation tests, temperature) exhibit strong temporal
491 dependence.

492 C.2 LLM Verification Results

493 To validate our independence test findings, we employed large language models for additional
494 verification. The detailed outputs from both Gemini and GPT models are presented below.

495 **LLM Analysis.** Figures 5 and 6 show the comprehensive LLM evaluation results for feature
496 independence assessment.

497 D Additional Relevance Test Results

498 We analyzed which clinical measurements contribute most to model predictions, independent of
499 temporal context. For each measurement, we computed the average feature importance across the
500 entire dataset and identified the top 10 most influential features:

501 INFLUENZA B, NUR1373, ALBUMIN, POC16, KETONE: URINE (UA), SARS-COV-2 RNA,
502 MYCOPLASMA PNEUMONIAE, POC:KETONE, POC:GLUCOSE BY METER, MAGNESIUM.

503 **LLM Analysis.** We show the llm outputs for feature relevance test in Figure 7 and 8.

504 E Prompt

505 We provide the prompts used to verify our model analyses using large language models (LLMs),
506 specifically Gemini 2.5 Pro and GPT-5 Mini.

507 **Independence Test Prompt.** This prompt is designed to verify the results of the independence test,
508 assessing whether features are statistically independent. The full prompt is shown in fig. 9.

GPT-5 mini

Measurements with High Temporal Correlation

- **LABPTT (3856):** Specific studies documenting its temporal correlation with sepsis are limited, but coagulation-related markers like PTT are generally relevant in sepsis monitoring.
- **GLOBULIN (728):** Direct evidence of temporal correlation in sepsis is sparse, though globulin levels reflect immune response changes.
- **WAM DIFTYP (6859):** No widely cited studies link this specific measurement to temporal sepsis prediction.

Measurements with Low Temporal Correlation

- **EKG5 (46):** Limited documentation of temporal correlation to sepsis; specific cardiac waveform features may vary in predictive value.
- **AST (SGOT) (166):** While AST can indicate organ dysfunction, temporal patterns in sepsis prediction are not well-established.
- **PLATELET COUNT (PLT) (2153):** Platelet count is relevant to sepsis prognosis, but temporal correlation in published literature is limited.
- **LYMPHOCYTE % (AUTO DIFF) (2281):** Lymphocyte percentage is a marker of immune status, but temporal effects for sepsis prediction are not clearly documented.

Figure 6: Feature temporal correlation analysis for sepsis prediction using ChatGPT-5 Mini. Features are categorized into High, Moderate, and Low time-correlated groups, reflecting progression markers, intermediate trends, and condition markers, respectively, as verified using the prompt shown in fig. 9.

Gemini 2.5 pro

Pathogens and Infectious Triggers Sepsis is fundamentally a dysregulated host response to an infection. Therefore, identifying the causative pathogen is a powerful predictor.

- **SARS-COV-2 RNA, INFLUENZA B, and MYCOPLASMA PNEUMONIAE:** These directly identify the infectious agent. Severe viral infections (like COVID-19 and Influenza) can lead to viral sepsis or predispose a patient to a secondary bacterial infection. Atypical bacteria like *Mycoplasma pneumoniae* are common causes of pneumonia, which is a leading trigger for sepsis.

Core Biomarkers of Systemic Illness These lab values reflect the widespread physiological chaos caused by the septic response, such as inflammation, metabolic derangement, and organ dysfunction.

- **ALBUMIN:** Low albumin (hypoalbuminemia) is a classic and very strong predictor of poor outcomes in sepsis. It reflects the severity of the systemic inflammatory response and a state of negative protein balance.
- **POC:GLUCOSE BY METER:** High glucose (stress hyperglycemia) is extremely common in critically ill patients. It's a result of the body's stress response and is associated with worse outcomes in sepsis.
- **POC:POTASSIUM and MAGNESIUM:** Electrolyte abnormalities are hallmarks of organ dysfunction in sepsis, particularly Acute Kidney Injury (AKI).
- **KETONE: URINE (UA):** The presence of ketones can indicate metabolic acidosis, a sign of severe metabolic stress and shock.

Figure 7: Feature influence analysis on sepsis prediction using Gemini 2.5 Pro. Features are categorized into High, Moderate, and Low influence based on their impact on model predictions, as verified using the prompt shown in fig. 10.

509 **Relevance Test Prompt.** This prompt is used to verify the results regarding the influence of each
510 feature, evaluating their impact on the model's predictions. The full prompt is shown in fig. 10.

GPT-5 mini

Features with Established Importance

- **Influenza B:** While specific studies on Influenza B's role in sepsis prediction are limited, respiratory viral infections, including influenza, have been associated with sepsis. Differentiating between influenza and *Mycoplasma pneumoniae* infections using peripheral blood routine parameters has shown diagnostic value, with an AUC of 0.845.
- **Albumin:** Hypoalbuminemia is a recognized marker of systemic inflammation and poor nutritional status, both relevant in sepsis. Low albumin levels have been linked to increased mortality in sepsis patients.
- **SARS-CoV-2 RNA:** COVID-19 has been associated with sepsis in some patients. Laboratory abnormalities in COVID-19 patients, particularly in coagulation function, have been related to the occurrence of sepsis.
- **Mycoplasma pneumoniae:** This pathogen can cause respiratory infections that may progress to sepsis. Studies differentiating influenza and *Mycoplasma pneumoniae* infections show its diagnostic relevance.
- **POC: Potassium:** Electrolyte imbalances, including abnormal potassium levels, are common in sepsis and can impact cardiac and muscular function.
- **POC: Glucose by Meter:** Hyperglycemia is frequently observed in sepsis and is associated with worse outcomes. Elevated blood glucose levels are primary risk factors for poor outcomes in various conditions.
- **Magnesium:** Hypomagnesemia has been linked to increased mortality in sepsis patients, suggesting its potential role as a prognostic marker.

Features with Limited or Unclear Importance

- **Ketone: Urine (UA):** While ketonuria can indicate metabolic disturbances such as diabetic ketoacidosis, its role in sepsis prediction is not well-established in the literature.

Figure 8: Feature influence analysis on sepsis prediction using ChatGPT-5 Mini. Features are categorized into High, Moderate, and Low influence based on their impact on model predictions, as verified using the prompt shown in fig. 10.

Prompt

You will be provided with results from our explainability method, which categorizes features based on their temporal correlation into three groups: High Time-Correlated Features, Moderate Time-Correlated Features, and Low Time-Correlated Features.

For each feature:

- Indicate whether you agree that the feature belongs in its assigned temporal correlation group.
- Briefly justify your agreement or disagreement based on reasoning about temporal patterns.

Here are the feature groups:

Figure 9: Prompt template for verifying feature temporal correlation group assignment.

Prompt

You are an expert in sepsis prediction. We have categorized features based on their impact on sepsis prediction into High, Moderate, and Low influence.

For each feature:

- Indicate whether you agree with the feature's assigned impact group.
- Briefly justify your agreement or disagreement based on reasoning about its role in sepsis prediction.

Here are the features:

Figure 10: Prompt template for verifying feature influence on sepsis prediction.